BioPhotonics workstation: A versatile setup for simultaneous optical manipulation, heat stress, and intracellular pH measurements of a live yeast cell

Aabo, Thomas; Bañas, Andrew Rafael; Glückstad, Jesper; Siegumfeldt, Henrik; Arneborg, Nils

Published in:
Review of Scientific Instruments

Link to article, DOI:
10.1063/1.3625274

Publication date:
2011

Document Version
Publisher's PDF, also known as Version of record

BioPhotonics workstation: A versatile setup for simultaneous optical manipulation, heat stress, and intracellular pH measurements of a live yeast cell

Thomas Aabo,[1] Andrew Raphael Banás,[2] Jesper Glückstad,[2] Henrik Siegumfeldt,[1] and Nils Arneborg[1]
[1]*Department of Food Science, University of Copenhagen, 1958 Frederiksberg C, Denmark*
[2]*Department of Photonic Engineering, DTU Fotonik, Technical University of Denmark, 2700 Kgs. Lyngby, Denmark*

(Received 20 April 2011; accepted 25 July 2011; published online 22 August 2011)

In this study we have modified the BioPhotonics workstation (BWS), which allows for using long working distance objective for optical trapping, to include traditional epi-fluorescence microscopy, using the trapping objectives. We have also added temperature regulation of sample stage, allowing for fast temperature variations while trapping. Using this modified BWS setup, we investigated the internal pH (pH_i) response and membrane integrity of an optically trapped *Saccharomyces cerevisiae* cell at 5 mW subject to increasing temperatures. The pH_i of the cell is obtained from the emission of 5-(and-6)-carboxyfluorescein diacetate, succinimidyl ester, at 435 and 485 nm wavelengths, while the permeability is indicated by the fluorescence of propidium iodide. We present images mapping the pH_i and permeability of the cell at different temperatures and with enough spatial resolution to localize these attributes within the cell. The combined capability of optical trapping, fluorescence microscopy and temperature regulation offers a versatile tool for biological research. © *2011 American Institute of Physics*. [doi:10.1063/1.3625274]

I. INTRODUCTION

Fluorescence microscopy is an important tool for biological research. In addition to viewing structural features, available via optical microscopy, supplementary information such as chemical composition or temperature can be mapped using fluorescent probes. Recently, it was used in whole-cell patch-clamp recordings from neurons transfected with a plasmid encoding green fluorescent protein tagged (GFP-tagged) mutant to measure ionic currents in response to two-photon illumination.[1] It can be used to assess cell health using fluorophores that have specific reactions to known biochemical indicators. Some fluorophores absorption or emission spectra also vary depending on the concentration of a specific ion, e.g., H^+, Ca^{2+}, Na^+,[2–4] in which case, the emission ratio between different wavelengths can be an indicator of the sample's chemistry. In addition to static chemical content, dynamic microscopic phenomena such as the interplay of chemical and thermal effects in biological samples is also interesting to observe with fluorescence microscopy. It is well known that temperature plays a major role on accelerating chemical reactions, imparting stress on organisms, and other biochemical reactions.[5] However, because of acquisition requirements, fluorescence microscopy cannot be used immediately to observe high temperature behavior. Heating is well known to cause thermal expansion and agitation, whereas fluorescence microscopy setups require samples to be stationary over the exposure time. A possible solution is to limit the working temperature ranges such that thermally induced motion is minimized. This, however, limits the dynamic behavior being observed. Another option is to shorten the exposure time. But with less time to capture the faint amount of emitted photons, such an option reduces image quality (signal to noise ratio).

Since the work of Ashkin,[6] optical trapping has been used in a variety of applications such as holding particles in place, micro-manipulation, and micro assembly.[7] A common trapping mechanism is to use tightly focused light to exert gradient forces on transparent objects such as dielectric particles and cells that refract light, causing change in optical momentum. Additionally, trapping also works with reflection based scattering forces as exploited by the BioPhotonics workstation's counter-propagating beams for axial positioning.[8] The effects of optical trapping on the health of cells had also been studied and is known to be small for certain wavelengths below certain power levels.[9–12] Thus, a trapping beam with minimal biological perturbance can be used to prevent thermal agitation in biological samples being observed with fluorescence microscopy.

To address the problems related to heating such as sample drift and possible damage to immersion objectives, we propose the use of long working distance optical trapping using the BioPhotonics workstation.[8] We investigate the internal pH (pH_i) response and membrane integrity of an optically trapped *S. cerevisiae* (baker's yeast) cell subject to increasing temperatures of up to 70 °C. We present fluorescence images showing the permeability and pH_i of the cell at different temperatures and with enough spatial resolution to identify which part of the cell has these attributes.

II. SYSTEM DESIGN

A. The BioPhotonics workstation

The BioPhotonics workstation (BWS) is an optical trapping platform designed to be extensible with its long

working distance and through side view imaging modalities.[8] This work extends the functionality of the BWS through traditional epi-fluorescence microscopy using the trapping objectives and by supporting a heating stage discussed in succeeding sections. The trapping module of the BWS has been previously described in detail.[8,13] Two independently addressable regions of a spatial beam modulating module are optically mapped and relayed as counter-propagating beam pairs in the sample. The trapping beams have a wavelength of 1070 nm and are operated at 5 mW. With conventional microscope setups, heating can cause drift to cells fixed to the surface since the chamber and stage experience thermal expansion. Thus, the stage needs to be adjusted continuously to compensate changes in the position and focus of the cell, thereby hindering high temporal resolution when imaging. By using optical traps to hold the cells away from the surface we obtain stable positioning of the cell, which is fixed with respect to the imaging setup and independent of stage movement. Thermal effects can also be a problem with high numerical aperture (NA) immersion lenses, as heat from the sample can cause condensation, expansion, or even damage to the objectives. The long working distances of the low NA objective lenses of the BWS prevent this problem caused by contact with the sample. The setup is able to support a heating stage and samples with a combined thickness of 4.3 mm, which can be heated and cooled rapidly and can maintain its set temperature. The low NAs also allow long range axial manipulation of trapped particles through counter propagating beam traps.[8] Such a feat cannot be done in optical tweezers relying on high NA focusing. The objective of this work is to show that even with this extra functionality, imaging through the BWS can still maintain the spatial and temporal resolution of a single cell.

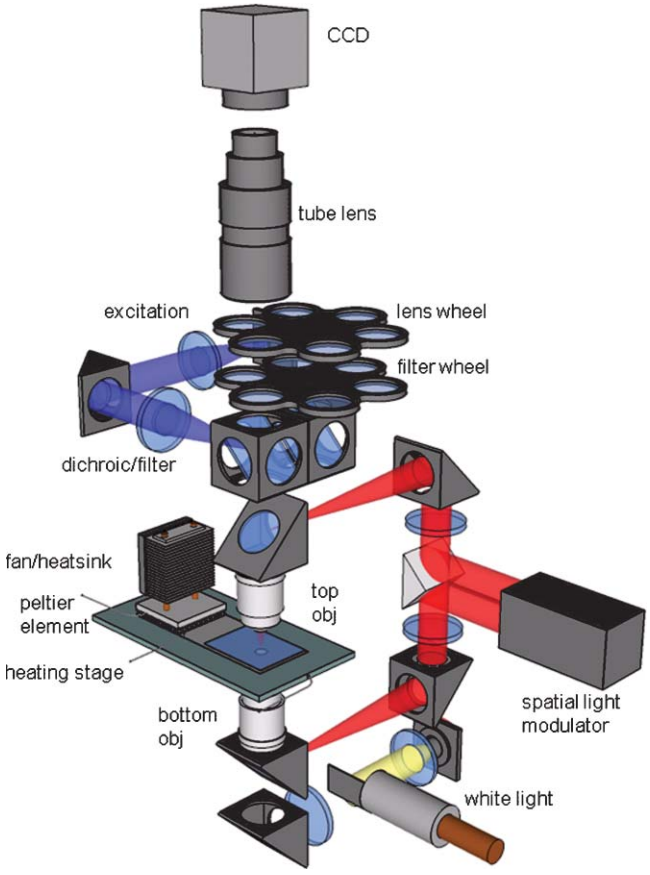

FIG. 1. (Color online) The BioPhotonics workstation modified to support a fluorescence setup and a heating stage. The same objectives used for counter-propagating beam traps (red) are also used for fluorescence imaging. The heating stage lies between the opposing objectives. Fluorescence light (blue) goes through the top objective through the dichroic mirror and passes through filters for imaging. White light (yellow) goes through the bottom objective for bright field illumination.

B. Fluorescence microscopy

The same objectives used for trapping in the BWS are also utilized for fluorescence imaging and bright field illumination. Figure 1 shows how the fluorescence setup is integrated with the BWS. A monochromator (Polychrome II, Till Photonics, bandwidth 15 nm) is used as the excitation light source. Changing the wavelength is automated with a LABVIEW program (see Sec. II D). Light from the monochromator is coupled to a quartz optical fiber (diameter 1.2 mm) and exits the fiber at an angle of 12.7° (NA 0.22). The light from the optical fiber is relayed through lens_1 ($f = 25.4$ mm) and lens_2 ($f = 150$ mm) then to the dichroic mirror block. Two dichroic blocks are used. Filter block 1 which is optimized for fluorescein and filter block 2, which is optimized, for propidium iodide. The switch between the two is done by simply moving the selected dichroic block into the optical path. The light is reflected by the dichroic mirror at an angle of 90° such that it is focused at the back focal plane of the top objective (Zeiss Plan-Neofluar, 40X, NA 0.75, WD 0.71 mm) of the BWS. This causes the light to be collimated upon reaching the sample plane, allowing a uniform excitation in the sample plane. Fluorescence emission from the sample goes back through the objective, then through the dichroic mirror, which can be interchanged through a sliding block mechanism. Light then goes through an emission filter, through the HOT mirror (Thorlabs, FM01). Before imaging, the emission light goes to an additional emission filter wheel where one of the following filters can be selected; an IR block (Schott, KG-5), an IR pass (Edmund optics, NT43–844) or no filter at all. Another wheel with 5 different lenses is used for ± 5 μm incremental changes in the z direction of the image plane. This allows focused imaging of cells trapped in different z-planes. Finally, fluorescence light goes through a tube lens (Olympus U-TV1X-2 Camera adaptor) and is then captured with a cooled CCD camera (Olympus QICAM with U-CMAD3 C-mount adapter ring JAPAN).

By placing the dichroic filters and emission filters in this way, the trapping module is unperturbed by the imaging system. This allows switching of filter blocks without any displacement or attenuation of the trapping beams. Due to the placement of the filters, the emitted fluorescence from the specimen is attenuated by the HOT mirror. The loss in intensity is, however, very small (<4%) (data not shown).

C. Fluorescent probes

The fluorescent probe used for pH_i measurements was 5-(and-6)-carboxyfluorescein diacetate, succinimidyl ester, (CFDA-SE) (Invitrogen C1157). The fluorescent active part of this molecule is fluorescein. This fluorophore has an absorption spectrum, which is dependent on the pH. The fluorophore is excited with two different wavelengths; i.e., 435 nm and 485 nm, where 435 nm absorption is relatively independent of pH and 485 nm absorption is more pH dependent. The ratio between the intensities is an indication of the pH.[14] Fluorescence ratio imaging microscopy utilizes this to determine spatial measurements of pH_i. This is done by taking two images at excitation wavelengths of 435 and 485 nm. The background intensity is subtracted. A ratio image is then created by dividing the intensity of the 485 nm image by the 435 nm image. The ratio image is then a representation of the spatial pH distribution.

To assess the membrane permeability the probe propidium iodide (PI) (Invitrogen C1637) was used. PI is an intercalating agent and attaches into double stranded DNA, and becomes fluorescent as it intercalates. The probe cannot cross intact cell membranes and will therefore only stain cells that have a compromised membrane.[15] PI has an absorption maximum around 530 nm, which is far above the absorption maximum of CFDA-SE. The two spectra are therefore far enough apart to enable us to load simultaneously and measure both probes in a single cell.

D. Monochromator and camera automation

Images are acquired at bright field illumination and different fluorescence excitation wavelengths for post processing. Acquisition from the CCD camera and selection of excitation wavelengths from the monochromator are automated with a LABVIEW (version 8.5) program (National Instruments). First, the wavelength of the monochromator (λ_1 = 435 nm, isosbestic wavelength of CF-SE) is set, then switched on, while the white light is switched off through their respective shutters. The exposure time of the camera is changed (1 s) and then a fluorescence image is captured. The wavelength is then changed (λ_2 = 485 nm, pH sensitive wavelength of CF-SE). The exposure time is changed (0.25 s) and another image is captured. Finally, the monochromator is switched off, the white light is switched on, and the camera exposure is reset to capture a bright field image (0.1 s). This sequence is repeated after a set interval to monitor temporal behavior with increasing temperature. In order to acquire the propidium iodide signal the dichroic filter block is switched from filter block 1 to filter block 2, the white light is shut off and the fluorescence wavelength is then changed again (λ_3 = 535 nm, propidium iodide absorption maximum) and the exposure time is changed to 0.1 s and the fluorescence image is captured.

E. Sample stage with temperature control

The heating stage for the sample is placed between the opposing objectives of the BWS. The stage is made up of an aluminum block and is thermally isolated with a plastic mount. Heat is introduced to the block with a peltier element (25 × 25 × 3.8 mm, Imax 2.2, Vmax 15, PE-127–08-15, Supercool) controlled by a control board (Supercool, PR-59). The PR-59 has a temperature resolution of 0.05 °C. Temperatures in the block are monitored with a thermocouple (Epcos, B57550G0503J). Another thermocouple (Epcos, B57540G0503J) is placed inside the sample for calibration. The resistance tolerance for both thermocouples is ±1% which translates to ±0.2 °C at 25 °C and ±0.8 °C at 70 °C. A heat sink and fan, normally used for computer processors, is used to prevent heat from building up. To prevent vibrations, the fan is not mounted to the heat sink but is supported by the base plate of the setup. When heating the aluminum stage, it expands resulting in movement mainly in the x-direction and a small movement in the z direction (data not shown). Optical trapping, however, keeps the cells fixed with respect to imaging. Once a stable temperature is reached, the chamber position does not significantly drift in any direction (data not shown).

The temperature of the stage is adjusted using a standard proportional-integral-derivative (PID) algorithm using SUPERCOOL software, controlling the peltier element. The method used is the standard Zeigler-Nichols method.[16] Optimization of the parameters is done so that the setpoint temperature is reached without an overshoot. The PID formula used is

$$U(k+1) = K_p e(k) + K_i \sum_{i=1}^{k} e(t_i)\Delta t + K_d \frac{e(t_k) - e(t_{k-1})}{\Delta t}, \quad (1)$$

where U is the current applied to the peltier element. $e(k)$ is the difference between the setpoint temperature and the measured temperature. The time increment, Δt, is 0.05 s. The 3 parameters K_p, K_i, and K_d controlling the proportional, integral, and derivative parts, respectively, are chosen such that minimal overshoot occurs and that the temperature remains stable. The resolution of the PR-59 controller insures that the temperature does not drift more than 0.05 °C, before the PID algorithm starts to reacts and adjusts the current to the peltier element in order to reach the setpoint temperature again. In practice, this will result in temperature variations no more than 0.1 °C once the setpoint has been reached.

F. Calibration of heating stage

It was necessary to determine the temperature differences between the stage and the sample chamber into which the cells are loaded. A small thermocouple (diameter = 0.8 mm, Epcos B57540G540) was inserted into a sample chamber filled with water and sealed with vacuum grease. The sample chamber with the thermocouple was placed on the stage and the stage was equilibrated to ambient temperature. Then, the setpoint was at first set to the ambient temperature (26 °C). After 1 min the setpoint was set to 71 °C. The stage reached 71 °C in 1 min and 40 s without overshooting (Fig. 2). The sample chamber probe had a small lag of ~15 s but followed the stage closely and reached 70 °C in 2 min. Both the

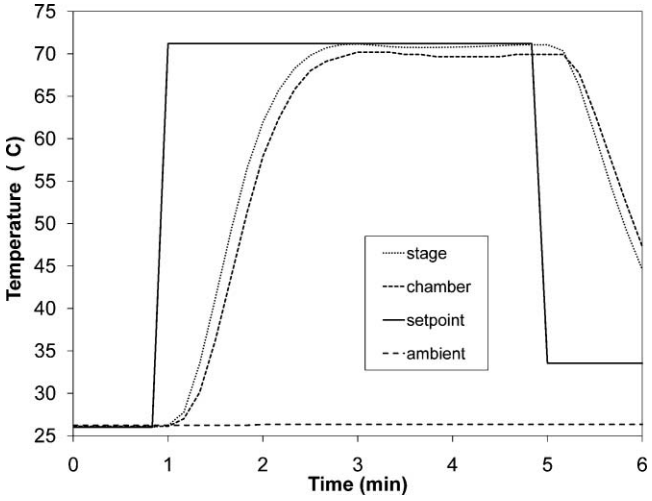

FIG. 2. Calibration of the heating stage. The temperature development of both the stage thermocouple (dotted line) and the sample thermocouple (dashed line). The solid line is the setpoint temperature, The dashed/square line is the ambient temperature.

stage and the sample chamber temperatures were stable, until the setpoint was changed after 5 min.

In order to reach the correct temperature in the sample chamber at different temperatures, it is necessary to calculate the correlation between the aluminum temperature (T_{Alu}) of the stage and the sample chamber temperature (T_{Cham}). In Figure 3, two parameters are plottet: the difference between aluminum temperature (T_{Alu}) and sample chamber temperature (T_{Cham}) ($\Delta T_{Alu\text{-}Cham} = T_{Alu} - T_{Cham}$), and the difference between aluminum temperature and ambient temperature (T_{Amb}) ($\Delta T_{Alu\text{-}Amb} = T_{Alu} - T_{Amb}$). Using a linear fit in Figure 3 given by

$$T_{Alu}(set) = C\,\Delta T_{Alu-Amb} + T_{Alu}, \tag{2}$$

we found a correlation factor $C = 0.028$, where $T_{alu}(set)$ is the setpoint temperature the stage should be set to in order to obtain the correct temperature in the sample chamber.

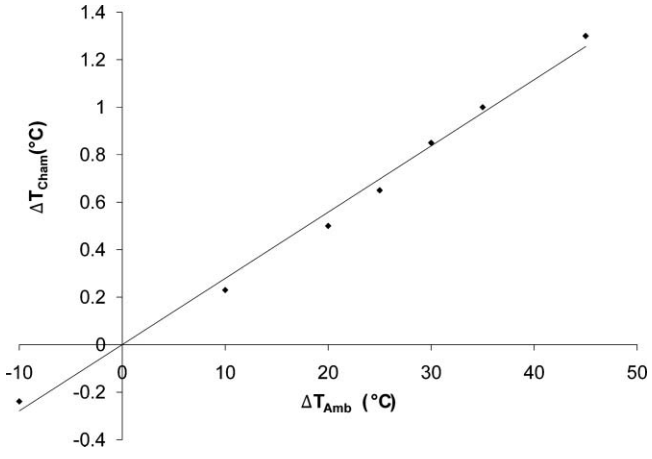

FIG. 3. Correlation between ΔT_{Cham} and ΔT_{Amb}. The slope of the linear fit is the correlation factor C.

III. EXPERIMENTS

The pH_i response and cell membrane integrity of a *S. cerevisiae* cell to increase temperatures was investigated while optically trapping it using a single trap with a power at the focus of 5 mW.

A. Staining and sample preparation

For heat stress experiments and calibration of pH_i, cells were grown at 25 °C under shaking (120 rpm) to exponential phase (OD = 0.1, 600 nm) in YPG medium (glucose 10 g/L, pH 5.6). The cell suspension (1 ml) was spun down and washed with pH 5.6 citrate/phosphate buffer (McIlvaine buffer).[17] The cells were then resuspended in the loading solution consisting of McIlvaine buffer (pH 7) and 40 μM CFDA-SE (from 4 mM stock in DMSO). The staining time of the cells consisted of incubation at 30 °C for 30 min. For heat stress experiments subsequently, the cells were spun down and resuspended in YPG medium (glucose 10 g/L) of pH 5.6 and 10 μM PI loaded into a sample chamber consisting of two 25 × 40 mm cover slips (Menzel-Gläser, #1, BB025040A1) separated by double-sided adheasive tape. The chamber was then sealed with silicone.

B. Calibration of pH_i

In order to correlate intensity ratios to pH it is necessary to create a calibration curve linking the fluorescence ratio to the pH. It is necessary for this to be done *in situ* as the spectral properties, as well as the pK_a may be affected by the internal environment of the cell.[18] The cells were grown to exponential phase and stained as stated above. The cells were then spun down and resuspended in 70% ethanol, which will rupture the membrane and equilibrate the pH_i and the external pH (pH_{ex}). The cells were then divided into the appropriate number of aliquots and resuspended in McIlvaine buffers ranging from pH 5 to pH 8. The cells were then loaded into chambers and ratio images were taken of the cells as described above. Figure 4 shows the calibration of *S. cerevisiae* cells at 8 different pH values. The data were fitted by a sigmoidal function given by

$$p\mathrm{H} = pK_a \left(\frac{R - R_{\min}}{R_{\max} - R}\right)^{1/s}, \quad R = \frac{I_{\lambda_1} - B_{\lambda_1}}{I_{\lambda_2} - B_{\lambda_2}} \tag{3}$$

where pK_a is the acid dissociation constant between the monoanion and dianion of carboxy fluorescein succinimidyl ester (CFSE).[19] $I_{\lambda 1}$ and $I_{\lambda 2}$ are the intensities collected from excitation with 435 nm and 485 nm, respectively, and $B_{\lambda 1}$ and $B_{\lambda 2}$ are the background intensities. R is the background corrected ratio between 435 nm and 485 nm excitation. R_{min} and R_{max} are the limiting ratio values of the high and low pH, respectively. S is the slope of the curve in the linear regime around the pK_a. The results from Fig. 4 are comparable to similar calibration curves in the literature.[11,20,23]

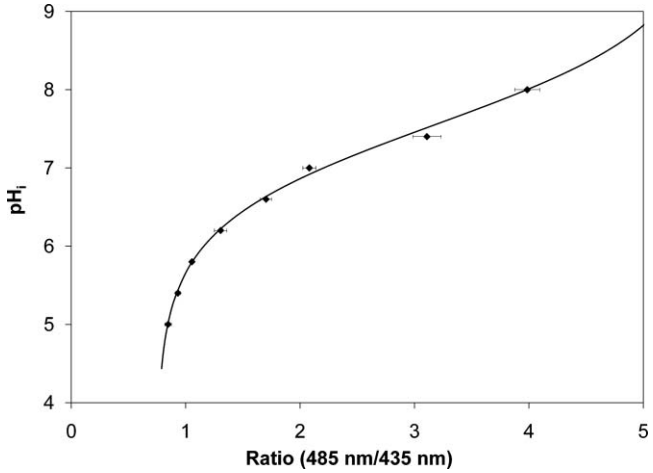

FIG. 4. The calibration curve between the emission ratio and the pH_i. Each data point is an average of 30 cells. The error bars represent standard error mean.

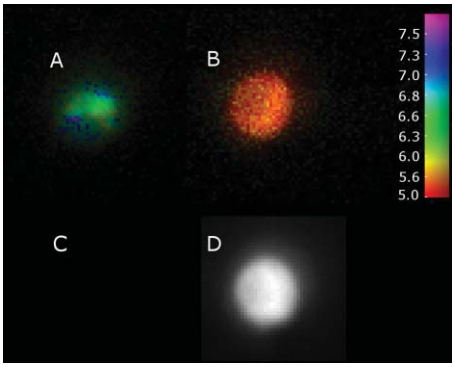

FIG. 5. (Color) Optically trapped single *S. cerevisiae* cell in YPG medium (pH 5.6). All four images are of the same cell. A and B show the pH distribution at t = 0 min (30 °C) and t = 12 min (70 °C), respectively. C and D are PI images at t = 0 min (30 °C) and t = 12 min (70 °C), respectively. The color bar represents pH values from 5 to 7.5. bar = 5 μm.

C. Heat stress of cells

A cell sample was made as stated in Sec. III A. A single *S. cerevisiae* cell was selected and trapped at 20 μm above the surface, and both the pH_i and membrane permeability of the single cell were measured. The chamber was then heated up to 70 °C at which it was held constant for 12 min. Fluorescence images were acquired as described in Sec. II C at t = 0 min (30 °C) and t = 12 min (70 °C). To ensure that the temperature difference itself did not influence the emission spectra, and thereby the pH measurement, additional images were afterwards taken at 30 °C. We did not find any difference in the ratio measurements due to temperature differences (data not shown). This is in line with other findings who only found a very small dependence of ratio measurements on temperature.[21]

Optical trapping of a cell will degrade the spatial measurements when acquiring an image, as the cell is not fixed to the surface but is trapped above the surface. This allows the cell some freedom to rotate within the trap. However, as the *S. cerevisiae* cells are not completely spherical and often a mother cell is coupled to its daughter cell, the cell will often find an equilibrium position along the z axis which is relatively stable. Provided that the exposure time of the camera is kept small (<1 s), this stable position enables us to acquire spatial information within the cell.

In Figure 5.A, we see cytosolic and vacuolar staining of the non-stressed cell with CFDA-SE even though the cell is optically trapped. We trapped the cell with a power of 5 mW. A t = 0 the cell has vacuoles with a pH of 6.3–6.6 and a cytosol with a pH of 6.8–7. This is comparable to values found in the literature.[22,23]. At t = 12 min after heat treatment, the pH_i drops to 5.6–5.7, and the pH is more homogeneous within the cell. The experiment was repeated 20 times. We found an average vacuolar pH of 6.5 ± 0.3 (SD) and cytosolic pH of 6.9 ± 0.2 when the cells were incubated at 26 °C. After the cells were exposed to 70 °C, the average pH value for the whole cell was 5.6 ± 0.1.

The loading of PI into the McIlvaine buffer allowed us simultaneously to look for membrane permeability in the same cell as a function of incubation temperature. In Figure 5.A, we see no staining of the non-stressed cell with PI, indicating that the membrane has not been ruptured and agreeing with the pH_i data in Figure 5.A. After 12 min of heat treatment we see intercalation of PI into the DNA (Figure 5.D). The staining indicates cell membrane rupture and correlates well with Figure 5.B, showing that $pH_i = pH_{ex}$.

IV. SUMMARY

This study reports on the development of a modified BWS setup enabling us to perform fluorescence imaging of a yeast cell kept stable by an optical trap while subjected to heat treatment at 70 °C. A trapping wavelength of 1070 nm and power of 5 mW was used. From the fluorescence images at 435 nm and 485 nm, we were able to measure the pH_i with CFDA-SE. Membrane permeability was assessed with the fluorescence from PI. Our results show enough spatial resolution within the cell while addressing heating problems such as drift due to thermal expansion and possible damage to immersion objectives. The combined capability of optical trapping, fluorescence microscopy, and temperature regulation of the modified BWS setup offers a versatile tool for biological research.

[1] E. Papagiakoumou, F. Anselmi, A. Bègue, V. De Sars, J. Glückstad, E. Isacoff, and V. Emiliani, Nat. Methods **7**, 848 (2010).
[2] T. Imai and T. Ohno, J. Biotechnol. **38**, 165 (1995).
[3] A. Minta and R. Y. Tsien, J. Biol. Chem. **264**, 19449 (1989).
[4] A. Minta, J. P. Kao, and R. Y. Tsien, J. Biol. Chem. **264**, 8171 (1989).
[5] G. M. Walker, *Yeast Physiology and Biotechnology* (Wiley, Chichester, 1998).
[6] A. Ashkin, Phys. Rev. Lett. **24**, 156 (1970).
[7] K. Dholakia, P. Reece, and M. Gu, Chem. Soc. Rev. **37**, 42 (2008).
[8] H. Ulriksen, J. Thogersen, S. Keiding, I. R. Perch-Nielsen, J. S. Dam, D. Z. Palima, H. Stapelfeldt, and J. Gluckstad, J. Eur. Opt. Soc. Rapid Publ. **3**, 080341 (2008).
[9] K. C. Neuman, E. Chadd, G. Liou, K. Bergman, and S. M. Block, Biophys. J. **77**, 2856 (1999).
[10] H. Liang, K. T. Vu, P. Krishnan, T. C. Trang, D. Shin, S. Kimel, and M. W. Berns, Biophys. J. **70**, 1529 (1996).
[11] M. B. Rasmussen, L. B. Oddershede, and H. Siegumfeldt, Appl. Environ. Microbiol. **74**, 2441 (2008).

[12]T. Aabo, I. R. Perch-Nielsen, J. S. Dam, D. Z. Palima, H. Siegumfeldt, J. Glückstad, and N. Arneborg, J. Biomed. Opt. **15**, 041505 (2010).
[13]D. Palima, T. B. Lindballe, M. V. Kristensen, S. Tauro, H. Stabelfeldt, S. R. Keiding, and J. Glückstad, J. Opt. **13**, 044013 (2011).
[14]M. M. Martin and L. Lindqvist, J. Lumin. **10**, 381 (1975).
[15]K. H. Jones and J. Senft, J. Histochem. Cytochem. **33**, 77 (1985).
[16]J. Ziegler and N. Nichols, ASME Trans. **64**, 759 (1942).
[17]T. C. McIlvaine, J. Biol. Chem. **49**, 183 (1921).
[18]P. Breeuwer and T. Abee, J. Microbiol. Methods **39**, 253 (2000).
[19]G. Bright, G. Fisher, J. Rogowska, and D. Taylor, *Methods in Cell Biology: Fluorescence Ratio Imaging Microscopy* (Academic, New York, 1989), pp. 157–192.
[20]D. Bracey, C. D. Holyoak, G. Nebe-von Caron, and P. J. Coote, J. Microbiol. Methods **31**, 113 (1998)
[21]R. Sjoback, J. Nygren, and M. Kubista, Spectrochim. Acta, Part A **51**, L7 (1995).
[22]R. Orij, J. Postmus, A. Ter Beek, S. Brul, and G. J. Smits, Microbiology **155**, 268 (2009).
[23]J. Vindeløv and N. Arneborg, Yeast **19**, 429 (2002).